On the internal solids circulation rates in freely-bubbling gas-solid fluidized beds

Chemical Engineering Science 172 (2017) 395–406

Contents lists available at ScienceDirect

Chemical Engineering Science

journal homepage: www.elsevier.com/locate/ces

On the internal solids circulation rates in freely-bubbling gas-solid fluidized beds

J.A. Medrano, M. Tasdemir, F. Gallucci *, M. van Sint Annaland

Chemical Process Intensification, Department of Chemical Engineering and Chemistry, Eindhoven University of Technology, De Rondom 70, 5612 AP Eindhoven, The Netherlands

HIGHLIGHTS

- The amount of solids inside bubbles has been quantified for different conditions.
- Bubble fraction measured differs from theoretical correlations.
- A novel method to determine the wake parameter has been developed.
- The internal solids circulation has been quantified by solving the mass balance.
- A sensitivity analysis confirms the need to correct for the assumptions.

GRAPHICAL ABSTRACT

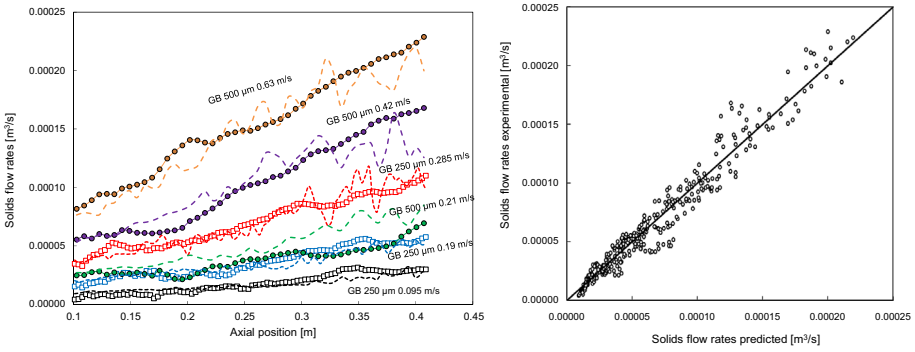

ARTICLE INFO

Article history:
Received 3 March 2017
Received in revised form 21 May 2017
Accepted 29 June 2017
Available online 30 June 2017

Keywords:
Fluidized bed
Assumptions
Hydrodynamics
PIV/DIA

ABSTRACT

The solids mass flux distribution and internal solids circulation rates in freely-bubbling gas-solid fluidized beds has been studied in detail in a pseudo-2D column. A non-invasive Particle Image Velocimetry (PIV) combined with Digital Image Analysis (DIA) technique has been further extended to investigate and quantify the gas and solids phase properties simultaneously for different particle types and sizes (all Geldart B type) at different fluidization velocities. It is found that the solids fluxes increase strongly, practically linearly, as a function of the vertical position and depend on the excess gas velocity but not on the particle size, while the most often used phenomenological two-phase fluidized bed models assume the vertical solids fluxes to be constant. To further investigate this important discrepancy, the underlying assumptions of the phenomenological models have been validated, especially concerning the average solids fraction inside the bubbles, the laterally and time-averaged axial bubble fraction profile (or visual bubble flow rate) and the wake parameter (the amount of solids carried along a bubble relative to the bubble volume). To this end, the PIV/DIA technique was further extended and a new method for the determination of the wake parameter is proposed. From the experimental results, it was concluded that i) the average solids fraction inside the bubbles is about 2.5–3% for glass beads and alumina particles and is practically independent of the excess gas velocity and particle size; ii) the measured laterally and time-averaged bubble fractions are considerably lower compared to often used correlations from literature, which would lead to a significant over-prediction of the visual bubble flow rate and iii) the wake parameter depends strongly on the bubble size and with the developed correlation the axial solids mass fluxes as a function of the vertical position can be well described. Finally, the influence of these findings was evaluated by performing a sensitivity analysis with an existing phenomenological model for fluidized beds with the new values and closures considering the case of the heterogeneously catalyzed steam methane reforming. With the developed findings and correlations the predictions with

* Corresponding author.
E-mail address: f.gallucci@tue.nl (F. Gallucci).

http://dx.doi.org/10.1016/j.ces.2017.06.046
0009-2509/

Nomenclature

Acronyms

CARPT	computed automated radioactive particle tracking
DIA	digital image analysis
ECT	electrical capacitance tomography
FCC	fluid catalytic cracking
MPT	magnetic particle tracking
MRI	magnetic resonance imaging
PEPT	positron emission particle tracking
PIV	particle image velocimetry
PTV	particle tracking velocimetry
Ar	Archimedes number
A_r	surface area of the column m^2
d_b	bubble diameter m
d_p	particle diameter m
SF	solids fluxes kg m^{-2} s^{-1}
u_0	superficial gas velocity m/s
u_{mf}	minimum fluidization velocity m/s
V_b	volume of the bubble cm^3
V_s	volume of the sphere cm^3

Greek letters

α	wake parameter
δ	bubble fraction in the bed
$\varepsilon_{bs,avg}$	average bubble solids holdup
ε_{mf}	emulsion phase porosity
ρ_g	gas density kg/m^3
ρ_p	particle density kg/m^3

the two-phase phenomenological models can be further improved, especially concerning the hydrodynamics of the solids phase.

1. Introduction

Fluidization technology is currently applied worldwide for many widely varying applications, ranging from chemical conversions, to polymer synthesis, adsorption, drying and many other processes (Kunii and Levenspiel, 1991). When the fluid flow is increased until the pressure gradient is overcome to suspend the particles, the solids phase assumes a fluid-like behaviour. In such conditions, the fluidized bed is considered at its minimum fluidization (u_{mf}) and with a further increase in the gas velocity bubbles start to appear. The behaviour of these rising bubbles are responsible for the main advantages of fluidized beds over other systems, as they induce the movement of particles creating efficient contact between the fluid and solid phases and vigorous mixing, which in its turn provides enhanced heat and mass transfer and thermal homogeneity.

A large-scale description of such a complex system has been proposed through phenomenological models that can be distinguished into different levels depending on the complexity and main underlying assumptions and correlations used (Horio and Wen, 1977; Kato and Wen, 1969; van Deemter, 1961; Kunii and Levenspiel, 1968). In general, the bubble phase refers to the voids rising in the bed, while the dense phase is referred to as emulsion phase. These models combine information on the hydrodynamics and bubble-to-emulsion mass transfer and describe the properties of the two phases along the bed height. Many of these properties have been studied, often separately, using various different experimental techniques, such as X-ray (Maurer et al., 2015), Particle Image Velocimetry (PIV) Bokkers et al., 2004, Digital Image Analysis (DIA) Lim and Agarwal, 1990, Particle Tracking Velocimetry (PTV) Chaouki et al., 1997, Magnetic Resonance Imaging (MRI) Boyce et al., 2014, Positron Emission Particle Tracking (PEPT) Laverman et al., 2012, Computed Automated Radioactive Particle tracking (CARPT) Fraguío et al., 2007, Electrical Capacitance Tomography (ECT) Weber and Mei, 2013, Magnetic Particle Tracking (MPT) Buist et al., 2014, electrostatic probes (He et al., 2015), or pressure sensors (van Ommen et al., 2011). Although the mass exchange between the gas in the bubbles and the emulsion phase has been investigated with different experimental techniques, the theoretical simplified approach described by Davidson and Harrison (1963) in the early 60's is still generally employed, with the improvement proposed by Kunii and Levenspiel (1991). To close the phenomenological models several assumptions have to be made, which have not all been validated by detailed experimental work. For instance, it is still often assumed that all excess gas above u_{mf} goes to the bubble phase and that the gas velocity in the emulsion phase remains constant at u_{mf} (i.e. assuming the visual bubble flow rate parameter to be equal to unity), that the solids are moving upwards in the wake of the bubbles at the corresponding bubble velocity and emulsion porosity with a constant wake fraction compared to the bubble volume, and that the bubble phase is free of particles. In this work some of these assumptions are revisited with new experimental data using a modern non-intrusive optical technique, in particular focusing on the amount of solids inside bubbles, and the bubble hold-up and wake fraction along the bed height.

Based on the postulate by Davidson and Harrison, a gas bubble is often assumed devoid of particles (Davidson and Harrison, 1963). Even though the solids volume fraction inside bubbles might be small, they could enormously influence practical operations where rapid kinetic operations are carried out. For instance, for mass transfer limited systems, and/or in case of highly exothermic catalytic reactions, where the catalytic particles may ignite inside bubbles of fresh reactant, resulting in changed selectivity or progressive deterioration of the catalyst. The solids content in the bubble phase has been investigated by different researchers using different techniques. Toei et al. (1965) photographed bubbles using a lens with an extremely shallow depth of field, while Hiraki et al. (1965) used the Tyndall effect of dispersed particles illuminated by a thin beam of light and Kobayashi et al. (1965) measured the bulk density of rising bubbles with a sensitive micro photo-transistor. In average, a solids content of 0.2–1.0% in the bubble phase was measured. More recently, Aoyagi and Kunii (1974) used a rapid combustion technique of dispersed particles by injected bubbles of air into a very hot bed of carbon particles fluidized at u_{mf} by air or nitrogen, using the fact that any particle finding itself in the air bubble ignites and becomes white hot and visible. Cui et al. (2000) investigated using a single cross-optical fiber probe the influence of different particle types (FCC catalyst and irregular sand) on the solids content inside the bubbles. They found that the

particle type largely influences the bubble solids holdup, where it ranges from 10–20% for FCC particles and 5–10% for sand particles. Andreux et al. (2005) investigated the solids holdup in the bubble phase using a combination of pressure measurements and a bi-optical probe in between the pressure sensors. They have found for sand particles an average of 5% of bubble solids holdup. Recently, Andreux and Chaouki (2008) measured the average solids fraction inside bubbles to be in the range of 8–12% using an intrusive bi-optical probe. Concluding, different experimental techniques have been used for the determination of bubble solids holdup in fluidized beds, where techniques using 2D beds achieve higher spatial resolution compared to techniques applied in 3D beds. The large discrepancy in the measured values for the solids content of the bubble phase warrants further investigation and possible validation of 2D and 3D techniques.

The solids vertical movement inside the bed is often described by considering a bubble wake phase that is carried upwards by the rising bubbles (Yang, 2003). This description applies for isolated bubbles, but is seriously thwarted for freely bubbling beds where frequent bubble coalescence and bubble splitting prevail. Nonetheless, in phenomenological models it is often assumed that (i) the wake has exactly the same velocity as the corresponding bubble and that (ii) the wake fraction is constant. While the first assumption is used to account for solids movement in the fluidized bed and to solve the material balance for the solids phase moving upwards and downwards (especially important in gas-solid reaction systems), the second one is more arbitrary and is based on analyses reported in the literature on the geometry of injected bubbles in an incipiently fluidized bed. The first studies on the wake characteristics were carried out by Rowe and Partridge (1965) in 1965. They reported that for bubbles in the size range from 2 to 10 cm, the wake parameter averages 25% of the total sphere volume depending on particle type and size. In 1973, Rowe and Widmer (1977) observed using X-ray photography that with increasing size of the bubbles, the wake parameter increases. This study was carried out by analysing bubbles in the size range between 1 and 16 cm for different combinations of flow rates, bed heights and powder material, and they proposed three different correlations to account for the variation of the bubble shape as a function of the bubble size, as presented in Eqs. 13 with V_b the bubble space volume (cm^3), V_s the sphere volume (cm^3), d_b the bubble diameter (cm) where α is the wake parameter.

$$\frac{V_b}{V_s} = 1 - \alpha = 1 - 0.0450 d_b \tag{1}$$

$$\frac{V_b}{V_s} = 1 - \alpha = 0.86 - 0.0180 d_b \tag{2}$$

$$\frac{V_b}{V_s} = 1 - \alpha = e^{-0.057 d_b} \tag{3}$$

Rowe and Widmer (1977) argued that all equations give a similar standard deviation on their data. However, Eq. (3) is proposed when working outside their data range as it is the most likely to give reasonable results. These equations give the ratio between the volume of a bubble and volume of a projected sphere from the visual spherical cap bubble, thus the remaining fraction is that of the wake. For really small bubbles in the range from 0.5 to 1.6 cm, Kozanoglu and Levy (1991) used a cylindrical fluidized bed where the bubbles rising adjacent to the transparent wall were recorded using a Videologic Instar video system. The individual images were analysed by hand by tracing the extended circle from the bubble, thus providing the theoretical boundary of the wake. These authors proposed a correlation for wake fraction based on the experimental conditions (Eq. (4)), although it is not commonly used as the range of bubble diameters where it is proposed for is very small.

$$\alpha = \left[(0.78 + 0.007 \cdot 6 d_p) + \frac{3899 d_b}{d_p^{1.103}}\right] / 100 \tag{4}$$

More recently, Mudde et al. (1994) analyzed the behaviour of a bubbling bed using images taken in a 2D bed. In their analysis, first spherical-cap bubbles were identified visually and subsequently the wake area was found by fitting another sphere to the rear of the spherical cap. The wake fraction is subsequently evaluated from the common area of the two spheres. They found that the wake fraction represents in average between 0.13 and 0.20 of the bubble volume with an average angle of the spherical cap bubbles of about 135–150°.

In almost all phenomenological models the wake parameter is assumed constant. In some recent models, such as in the work of Iliuta et al. (2010) and Gascon et al. (2006) typically a value of 0.15 is used for the wake parameter. However, in these works the fluidized bed was modelled for cases where the solids fluxes are not very important. In novel technologies like chemical looping processes, where a solid is continuously circulated between two interconnected reactors, the extent of the internal solids circulation is, however, of great interest and it strongly influences the solids conversion as well as the design and operation of the reactor, especially regarding the solids extraction and solids feeding points. Therefore, in this work a new method based on a solids mass balance throughout the bed is developed to calculate the wake fraction in the bubbling regime. This method provides a more realistic measurement of the wake parameter compared to studies based on the bubble geometry, since it takes the overall effects of bubble coalesce and bubble splitting on the mass fluxes into account.

The bubble fraction has a strong influence on the wake fraction and thus on the magnitude of the solids fluxes. In general, it is assumed that all excess gas above the minimum fluidization velocity goes to the bubble phase. Kunii and Levenspiel developed a theoretical description of the bubble fraction throughout the fluidized bed depending on the excess gas and the bubble rise velocity (Eq. (5)) Kunii and Levenspiel, 1991, that is often used, although the validity of this assumption might be questioned, as reported before in the literature (Hilligardt and Werther, 1986). This theoretical description of the bubble fraction is widely applied in phenomenological models since at large scales the bubbles are big and fast. In this work, this correlation is selected since from experimental data the measured bubble rise velocity (u_b) is 2–2.5 u_{mf}/ε_{mf}. In this work, also the theoretical correlation given in Eq. (6) could be applicable. In this work the correlation given in Eq. (5) is applied; it will not change the main findings. When using the assumption that the solids move in the wake phase with a velocity equal to the bubble velocity, and the correlation for the bubble fraction depicted in Eq. (5), together with the assumption of a constant wake parameter, the solids flux should not change along the vertical position, i.e. the solids are assumed to move in plug flow, as detailed in Eq. (7), where α is the wake parameter that relates the wake fraction to the bubble fraction (δ), u_b is the bubble rise velocity, ρ_p the particle density, ε_{mf} the gas porosity and A_R the surface area of the reactor:

$$\text{Bubble fraction for } u_b \approx 5u_{mf}/\varepsilon_{mf} \quad \delta = \frac{u_o - u_{mf}}{u_b} \tag{5}$$

$$\text{Bubble fraction for } u_b \approx u_{mf}/\varepsilon_{mf} \quad \delta = \frac{u_o - u_{mf}}{u_b + u_{mf}} \tag{6}$$

$$\text{Solid fluxes over the bed} \quad SF = \alpha\delta u_b \rho_p (1 - \varepsilon_{mf}) A_R = \alpha(u_0 - u_{mf})\rho_p(1 - \varepsilon_{mf})A_R \tag{7}$$

The objective of this work is to extend the existing novel experimental techniques (PIV/DIA) to study in detail some of these

assumptions that are widely adopted in the field of fluidization, and to subsequently investigate their influence on the performance of the phenomenological models to describe the conversion in a fluidized bed reactor. Contrary to previous investigations that were often based on theoretical descriptions or geometrical analyses, this work is based on the analysis of actual dynamics of a gas-solid fluidized bed in the freely bubbling regime. First the experimental setup and experimental conditions are presented. Subsequently, the novel methods developed for the analysis of the assumptions are described in detail. Finally, the results obtained in this work are presented and discussed, and the main conclusions obtained from this work are summarized.

2. Experimental methods

2.1. Experimental techniques

Particle Image Velocimetry (PIV) is a non-invasive measuring technique developed originally to investigate liquid or gas-liquid systems, but recently extended to gas-solid dispersed flows. The basic principle of PIV is to divide recorded images into $N \times N$ interrogation areas and use a spatial cross-correlation on two consecutive images, thus the instantaneous emulsion phase velocity of fluidized beds can be obtained. PIV was first applied in 2004 by Bokkers et al. (2004) to investigate emulsion phase circulation patterns and it was further extended to studies on fluidization regime maps (Link et al., 2005), granular temperature (Dijkhuizen et al., 2007), freeboard region (surface of a fluidized bed) (Duursma et al., 2001), bubble eruption (Müller et al., 2007) and particle behaviour (Pallarès and Johnsson, 2006).

The principle of Digital Image Analyses (DIA) is to record images of the fluidized bed with a high speed camera and use the pixel intensity to discriminate between the bubble and the emulsion phases, thus bubble properties can be measured. By taking consecutive images and using spatial cross-correlation techniques, the displacement of the centre of mass of bubbles can be determined. DIA was first performed in 1990 by Lim and Agarwal (1990) to study the bubble size, velocity distribution, and bubble hold-up distribution. Later DIA has been used to study bubble-wake acceleration (Agarwal et al., 1997), bed expansion and segregation rates (Goldschmidt et al., 2003), relations for bubble properties (Shen et al., 2004), local hold-up (Mudde et al., 1994), or bubble distribution and fluidized bed behaviour (Lim et al., 2007). Recently, both non-invasive optical techniques have been combined into one general technique (PIV/DIA) as proposed in 2012 by Laverman et al. (2008). With this technique the instantaneous emulsion phase velocity fields are obtained together with detailed information on the bubble phase (local bubble size and velocity distribution, bubble fraction etc.), which allows investigation of the mutual interactions in detail.

PIV-DIA is a non-invasive technique that requires the use of pseudo-2D fluidized bed columns to allow visual inspection of the dynamics of the bed. In this work a pseudo 2D column with the front wall made of glass and 1500, 300 and 15 mm in height, width and depth respectively, has been used. The back wall of the column is made of anodized black aluminium to enhance the optical detection of the particles. Air is used as gas phase and is fed into the column through a porous plate distributor with 40 μm average pore size and 1 cm in thickness. The volumetric gas flow rate is controlled via a 500 L/min mass flow controllers (Bronkhorst B.V. Instruments), which provides enough flow for a proper fluidization regime. Experiments have been carried out with different particles (type and size) and gas fluidization velocities (Table 1) to cover a wide range of operating conditions. For all the particles the experimental minimum fluidization velocity has been determined separately using the standard pressure drop method.

Two different image acquisition setups are used to investigate in detail all the assumptions of interest. To study the bubble fraction along the bed height, a high acquisition frequency is required in view of the high bubble velocity, for which a high-speed camera (Phantom v.341 from DantecDynamics) recoding at full resolution (2400×2400 pixels) and 100 frames per second is used. Homogeneous illumination throughout the bed is provided by four LED lights as depicted in the schematic representation in Fig. 1. On the other hand, the average solids fluxes and bubble properties are determined from recorded images using a "Dantec system Flowsense EO 16 M" camera, which provides a maximum resolution of 4300×3200 pixels. Experiments are carried out by recording a sufficiently long sequence of double exposure images with a

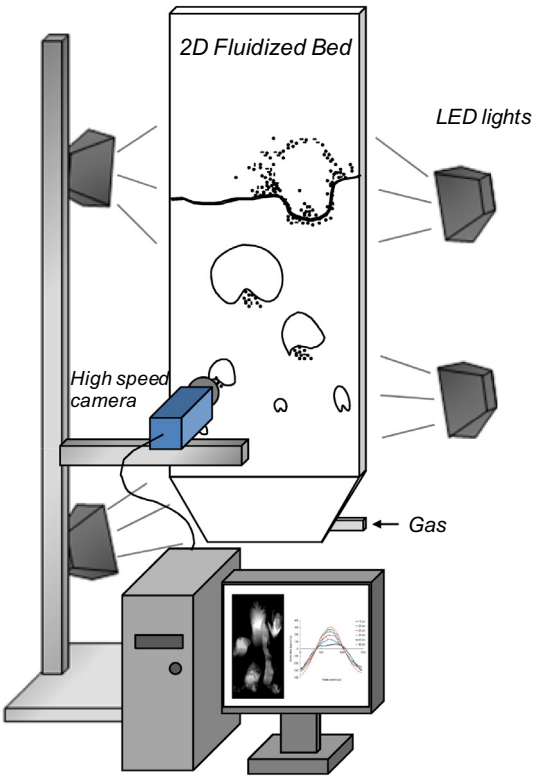

Fig. 1. Schematic representation of the experimental setup used in this work.

Table 1
List of experiments.

Particle	$d_{p,avg}$ [μm]	Geldart [–]	u_{mf} [m/s]	u_0/u_{mf} [–]
Glass beads	500	B	0.210	2, 3 and 4
Glass beads	250	B	0.090	2, 3, 4, 5, 6 and 7
Activated alumina	500	B	0.160	2, 3 and 4
Polyethylene	1015	B	0.330	2, 2.5 and 3

frequency of 2 frames per second. All images are taken at 2.5 pixels per particle in order for PIV to work optimally (Westerweel, 1997). The camera settings have been optimized to a time between the two exposures of 1 ms and 8 bit camera depth resolution. For the experiments, first the camera is aligned perpendicular to the column and the lens is focused for the detection of particles. Subsequently, the LED lights are evenly placed at different heights until homogeneous illumination is observed in the bed. Reproducibility has been assessed by repeating experiments on different days and after modifying the conditions of the setup.

2.2. Analysis methods

2.2.1. Solids content inside bubbles

The method proposed for measuring the amount of solids inside bubbles uses the correlation developed by de Jong et al. (2012) to obtain the 3D solids porosities (Fig. 2(A)) from 2D intensities. Subsequently, the image is divided into bubble and emulsion phases and the bubble phase image (Fig. 2(B)) is used as a mask on the initial image to obtain the solids hold-up in each pixel defined as bubble phase as depicted in Fig. 2(C).

Subsequently, the sum of the solids hold-up in the bubbles is divided by the total amount of pixels defined as bubbles to obtain the average bubble solids hold-up per image. This procedure can be repeated for n images as presented in Eq. (8)

$$\varepsilon_{bs,avg} = \left(\sum_n \frac{\sum \varepsilon_{bs,px,n}}{\sum px_{b,n}} \right) / n \tag{8}$$

The threshold value used for a bubble is a solids porosity of 0.20. However, this does not imply that anything below 0.20 should be considered as solids inside the bubbles. A histogram of the average frequency of the solids porosity inside the bubbles (Fig. 2D) reveals that 95% of the solids porosity values are between 0 and 0.10, while the remaining 5% (between 0.11 and 0.20) are considered as the edges between the emulsion and bubble phase and hence they are excluded in the analysis method. This method is applied to different particle types and at different excess gas velocities (u_0-u_{mf}).

2.2.2. Bubble fraction

The use of a high-speed camera allows bubble tracking throughout the bed, thus the effect that bigger bubbles rise faster than smaller ones is accounted for in the method. The developed method to determine the bubble fraction takes first slices at different axial positions and subsequently divides instantaneous images into bubble and emulsion phases throughout the bed. The sum of the pixels defined as bubble phase is divided by the total amount of pixels in that slice, thus obtaining the bubble fraction on that specific axial position. This procedure can be repeated up to n images as stated in Eq. (9), and the evolution of the bubble fraction as a function of n images is shown in Fig. 3. The bubble fraction has been measured using different particles and different excess velocities and results have been compared to the correlation by Kunii and Levenspiel (Eq. (5)) using the experimentally determined values of u_{mf} and u_b (time-averaged as a function of the vertical position in the bed)

$$\delta_y = \left(\sum_n \frac{\sum px_{y,b,n}}{\sum px_{y,n}} \right) / n \tag{9}$$

2.2.3. Wake parameter

In this study, the wake parameter is determined solely from the experimental results obtained with the PIV/DIA experimental technique. The required data are the bubble fraction (using the method developed in this work), bubble diameter, bubble rise velocity and solids fluxes. The novel method is based on the analysis of the average results obtained for the solids fluxes within the bed and combined with average bubble properties. PIV/DIA allows the measurement of the time and laterally averaged solids fluxes at every vertical position in the bed. First, the instantaneous velocity field of the emulsion phase is obtained from PIV (Fig. 4 (left) shows the time-average solids fluxes). Subsequently, the instantaneous solids porosity is obtained through DIA using the correlation suggested by de Jong et al. (2012) (Fig. 4 (centre) is the time-average solids porosity).

Finally, by combining the instantaneous velocity field of PIV (u_e) and the instantaneous solids porosity field from DIA (ε_s) at the different vertical positions, the instantaneous lateral solid fluxes per axial slice can be obtained as presented in Eq. (10), which is subsequently time-averaged. The resulting time-averaged lateral profiles of the vertical solids fluxes at different vertical positions is shown in Fig. 4 (right), where the sum of the positive fluxes should be equal to the sum of the negative fluxes to close the overall solids mass balance.

$$SF\left[\frac{kg}{m^2 s}\right] = u_e\left(\frac{m}{s}\right) \cdot \varepsilon_s \cdot \rho_s \left[\frac{kg}{m^3}\right] \tag{10}$$

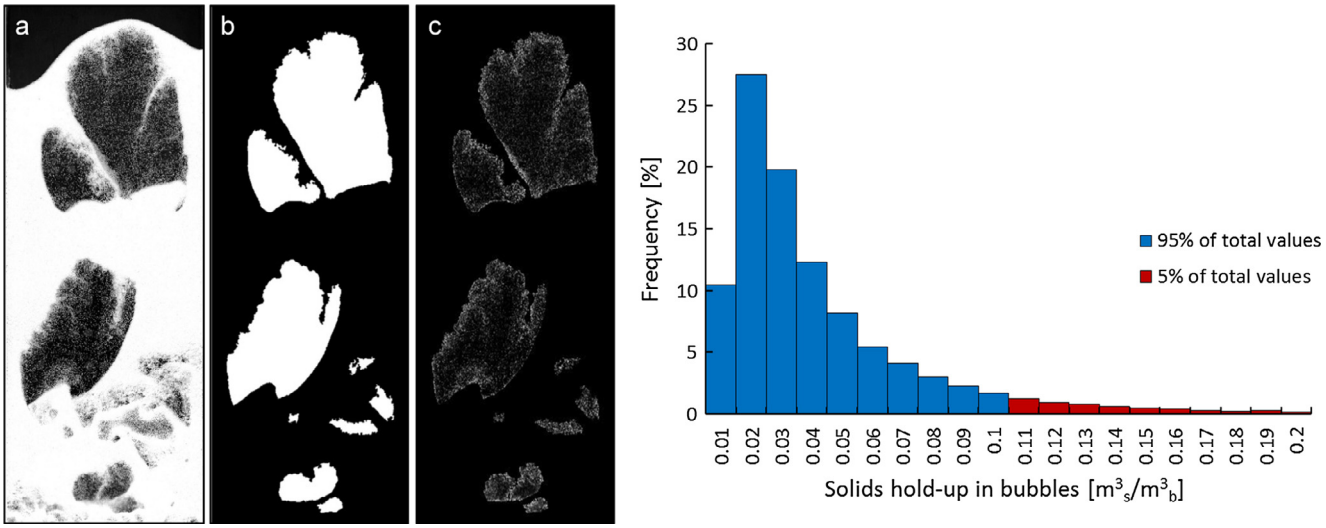

Fig. 2. From left to right (A) 3D porosity image, (B) bubble detection mask, (C) solids hold-up in bubbles, (D) histogram of the amount of solids inside bubbles.

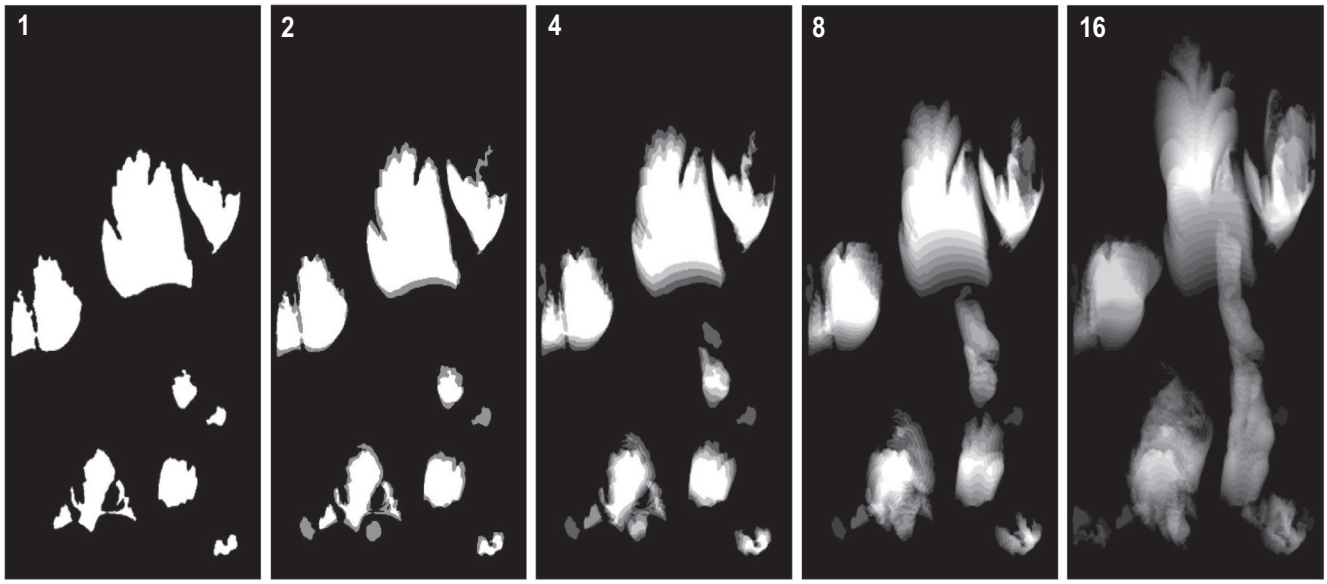

Fig. 3. Average bubble fraction for "n" images, from left to right "n" is 1, 2, 4, 8, and 16.

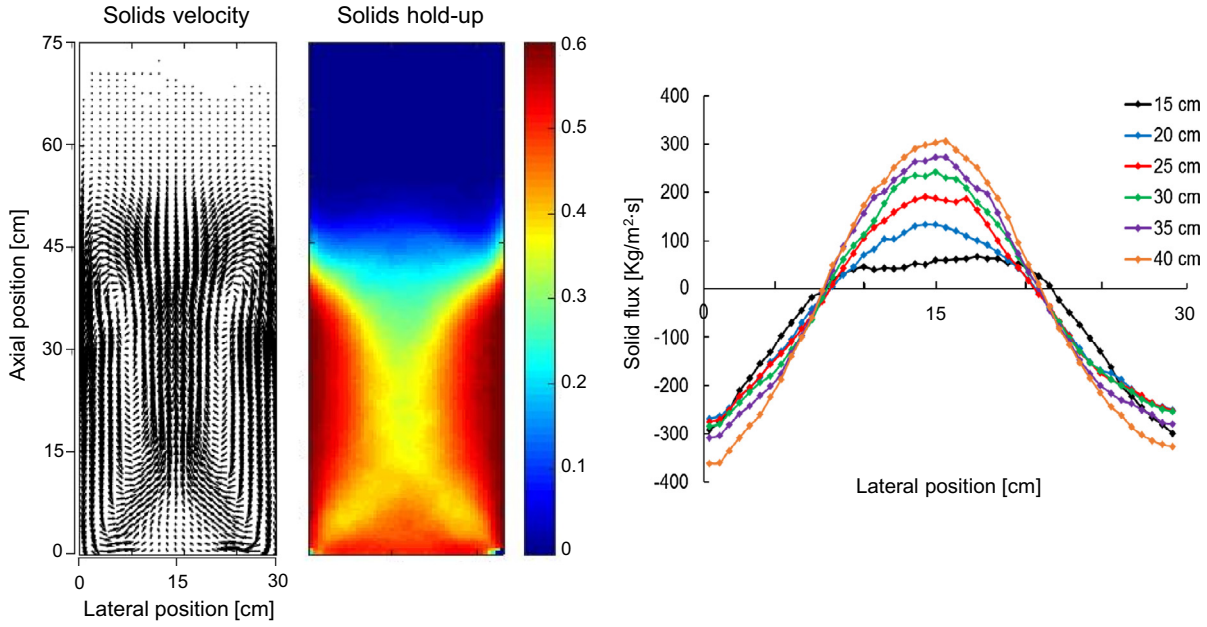

Fig. 4. Left (A) Average solid velocities in bed from PIV, centre (B) Average bed porosity from DIA and right (C) time-averaged vertical solid fluxes in bed in the lateral position at different heights.

The underlying assumption considered in this method (also commonly used in the literature) is the fact that the wake phase is responsible for transporting the solids upwards in the bed. Therefore, a mass balance (Equation (11)) can be written for the solids phase moving upwards in the bed, which should include the bubble rise velocity (u_b), the wake fraction of the bubble ($\alpha \cdot \delta$) and the solids holdup of the wake phase ($1-\varepsilon_{mf}$) that can be approximated to the solids holdup in the emulsion phase. Through this mass balance, the vertical solids fluxes can be calculated. Experimentally, the vertical solids fluxes are measured in PIV/DIA as a function of the vertical direction using the positives of the average lateral solids fluxes profiles as presented in Fig. 4c. From the lateral profiles, the area of the positive vertical solids fluxes represents the solids moving upwards in the bed [in kg/s], which is calculated using the trapezoid method and then converted into a volumetric flow rate [m^3/s].

$$SF_y = \alpha_y \cdot \delta_y \cdot u_{b,y} \cdot (1 - \varepsilon_{mf}) \cdot A_r \tag{11}$$

$$\varepsilon_{mf} = 0.586 Ar^{-0.029} \left(\frac{\rho_g}{\rho_p}\right)^{0.021} \tag{12}$$

Using only DIA, the upward volumetric flow rate could also be obtained as presented in Eq. (11). However, the value of the wake parameter (α) that relates the wake fraction to the bubble fraction (δ) is unknown. In this method, δ and the bubble rise velocity (u_b) are obtained from experimental results and ε_{mf} is the emulsion gas porosity that can be determined using Eq. (12) proposed by

Broadhurst and Becker (1975). Because the solids flow rates obtained from PIV/DIA (Eq. (10)) and the solids flow rate from Eq. (11) should be equal, the wake parameter α can be directly calculated in order to satisfy the identity and thus to solve the internal solids mass balance in the fluidized bed. This method to determine the wake parameter has been applied to different particle types, shapes and different excess gas velocities and the obtained results are compared to other wake parameter values and correlations presented in the literature. Note that in this work the solids movement has been related to the solids transport via the wake of the bubbles. This description applies well for cases of isolated bubbles in a large fluidized bed. However, for freely bubbling beds other phenomena may play a role the upward movement of particles, such as bubble-bubble interactions and the gas through-flow from bubble to bubble pushing the particles upwards. In phenomenological models these effects are often combined and lumped in the wake fraction since the through-flow rate is also proportional to the bubble diameter.

3. Results

3.1. Solids inside bubbles

In this work, the presence of solids inside bubbles has been experimentally determined for different particles according to the methodology previously described, and the results are represented in Fig. 5. The amount of solids inside bubbles ranges from ~1.5% to ~3.5%. There are small deviations for each particle type at different gas velocities, which might be related to differences in the particle densities. Relatively high density particles (glass beads) show a slightly decreasing trend in the bubble solids up at higher gas velocities, whereas low density particles (LDPE and porous alumina) show a slightly increasing trend. However, the changes at different gas velocities are rather small and as a first approximation one may assume that the solids hold-up inside the bubbles does not depend on the fluidization velocity and is about 2.5–3% for glass beads and alumina particles and somewhat lower (about 1.5%) for LDPE particles. The developed method does not allow the measurement of the bubble solids holdup per individual bubble, but does the determination per image. In theory, it could be expected that big bubbles would have a higher solids holdup than small bubbles. However, this variability cannot be determined with the current method. On the other hand, since the measurements are done per image, it is possible to determine the average standard deviation over the measurements for each particle type and fluidization conditions. This deviation is somewhat related to variability in bubble solids holdup since every image has a different bubble size distribution. The measured deviation ranges from ±20 to 25% for every condition and particle type.

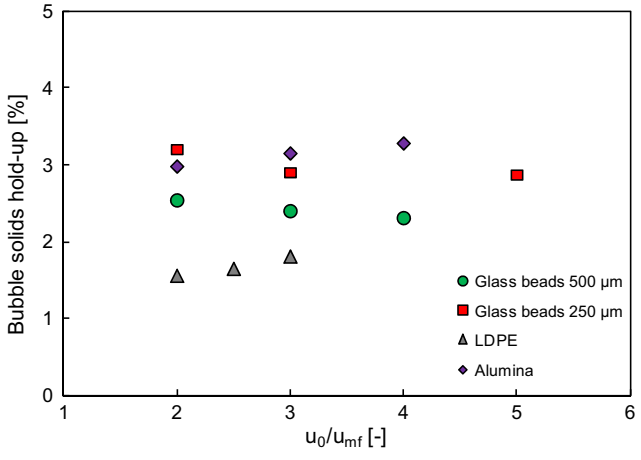

Fig. 5. Bubble solids hold-up as a function of u_0/u_{mf} for different particles. A standard deviation of ±20–25% has been measured for each particle type and fluidization velocity.

The values for the bubble solids hold-up are considerably higher than rough estimates reported in early literature (Toei et al., 1965; Hiraki et al., 1965; Kobayashi et al., 1965), which ranged from 0.2% to 1%, and significantly lower than other values recently proposed (Andreux and Chaouki, 2008). The early works were done in very thin beds with single injected bubbles and limited methods to convert the observed particles to porosity as opposed to this work. Moreover, the number of particles in the depth direction was also lower compared to this work and under these conditions the gas phase tends to bypass the emulsion phase near the walls and wall effects are more pronounced. This may explain the observed discrepancies. On the other hand, the work of Andreux and Chaouki (2008) is based on an intrusive optical technique with a low spatial resolution (3 mm in diameter), thus not able to provide complete information on the solids content inside the bubbles.

3.2. Bubble fraction

The experimental bubble fractions measured for glass beads with a $d_{p,avg}$ of 250 µm and at different u_0/u_{mf} are presented in Fig. 6 (left), whereas a comparison to the theoretical correlation proposed by Kunii and Levenspiel using the experimental data is reported in Fig. 6 (right). The comparison has been carried out for experiments at u_0/u_{mf} of 2, 3 and 5. Using the determined u_{mf} from pressure drop measurements and the time-averaged bubble rise velocity (u_b) for each case, the expected bubble fraction (δ) has been calculated based using the theoretical correlation proposed in Eq. (5). One should note that this correlation is thus used with the obtained experimental data.

Results show an increase in the bubble fractions at the bottom part of the column associated to the limitations of the PIV/DIA method. Bubbles smaller in diameter than the depth of the column (1.5 cm) cannot be detected, thus only when the average bubble diameter is sufficiently high the method picks up the actual bubble fraction. All trends stabilize and are fairly constant at an axial position of ~0.1 m and higher, where most of the smaller bubbles have coalesced into detectable larger ones. The measured bubble fractions are considerably lower compared to the calculated bubble fractions from the Equation proposed by Kunii and Levenspiel and using the experimental u_{mf} and u_b, thus indicating that the theoretical Equation overestimates the bubble fraction. This can be associated to two effects: i) the assumption that all excess gas goes to the bubble phase is inaccurate as already discussed in the literature (Hilligardt and Werther, 1986) and ii) the measured bubble rise velocity differs from the correlation used by Kunii and Levenspiel for their theoretical description, which is based on the findings of Davidson and Harrison (1963) for gas-liquid systems. Furthermore, it is observed that the determined bubble fraction using the experimental data in the theoretical correlation (Eq. (5)) gives values of bubble fraction above 1 at the bottom of the bed, which is associated to the difficulties of the used technique in tracking small bubbles. Therefore, the measurements below 0.10 m in bed height should be ignored. If Eq. (6) would have been used instead, the calculated bubble fractions (dashed lines) would slightly decrease, although they will still largely over predict the experimental findings.

As the obtained values for the bubble fraction are rather constant over the bed height above 0.1 m above the distributor, for subsequent calculations involving the bubble fraction, a power law equation (Eq. (3)) based on the average bubble fraction values from the constant part of the column is used.

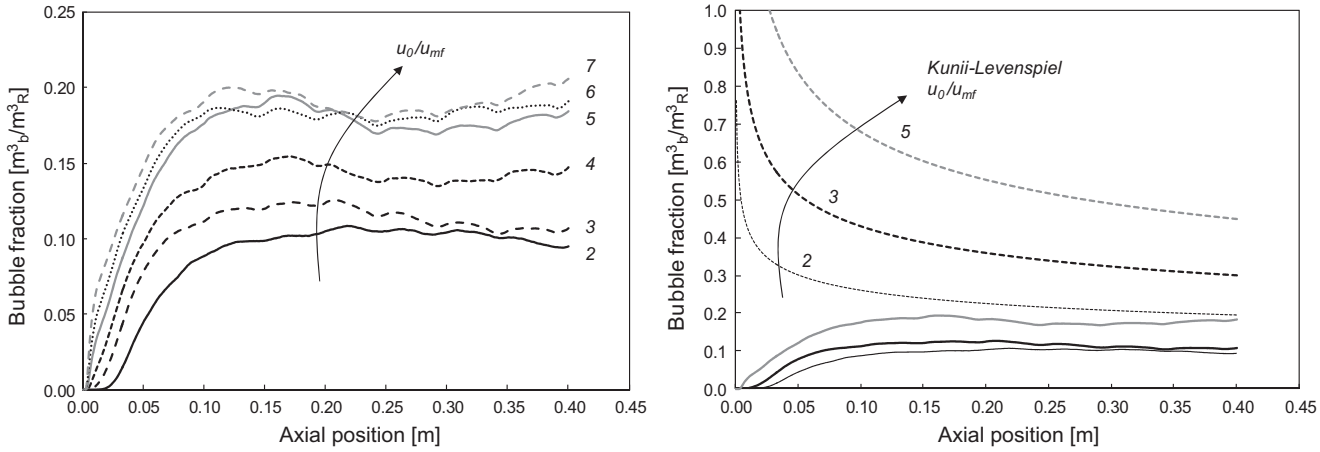

Fig. 6. Bubble fraction as a function of the vertical position for 250 μm glass beads and different u_0/u_{mf} (left) and comparison to theoretical bubble fraction from literature (Kunii and Levenspiel, 1991) (right), where dashed lines are obtained with the theoretical correlation and lines are the respective experimentally measured bubble fractions.

$$\delta = 0.24(u_0 - u_{mf})^{0.39} \tag{13}$$

It is generally assumed that the bubble fraction solely depends on the excess gas velocity and not on parameters such as the particle size, density or sphericity. However, this has not been investigated in detail in the literature. The fact that this method is based on a 2D imaging technique raises the question if it is suitable to extend to 3D beds. Because this method is based on pixels designated as bubble phase or as emulsion phase it is possible to extend it to 3D imaging techniques, such as X-ray tomography. Using a threshold value to distinguish bubbles and working at similar conditions, X-ray tomography on 3D beds can be used to validate this method for 2D beds. When confirmed, it is preferred to work with 2D imaging techniques due to reduced complexity, processing time, amount of data storage, and the increased spatial and temporal resolution.

3.3. Wake parameter

The solid flows for the different particle types investigated and at different gas velocities were obtained using the PIV/DIA method developed in this work. Because the PIV/DIA method has difficulties at the bottom of a fluidized bed due to the presence of small bubbles, the solid flows are evaluated from above an axial position of 0.1 m, which is the same height at which the bubble fraction was determined.

The determined time and laterally averaged solids flow rates for glass beads of 250 μm and 500 μm in diameter and for LDPE particles as a function of the vertical position in the bed at different excess gas velocities can be seen in Fig. 7. The results show strongly increased solids flow rates at higher vertical positions with an almost linear behaviour for all particle types and, remarkably, the solids flow rates are increased with increasing excess gas velocities. For instance, for the cases of 500 μm diameter glass beads with an excess gas velocity of 0.21 m/s and 250 μm diameter glass beads with an excess gas velocity of 0.19 m/s, the measured solids flow rates are very similar, thus indicating that for the same particle type the solids flow rate depends mainly on the excess gas velocity and not on the size of the particle (both Geldart B type particles). The LDPE particles also show a linear increase in the solids flow rates as a function of the vertical position for all excess gas velocities. This linearity for both the glass and polymer particles is quite surprising, as it implies that a constant wake parameter, by default, will not describe the system properly.

In the case of alumina particles, less defined trends are obtained compared to glass and polymer particles (Fig. 8). At an excess gas velocity of 0.162 m/s (u_0/u_{mf} of 2) the PIV/DIA technique has difficulties picking up the solids flow rates as the alumina particles are

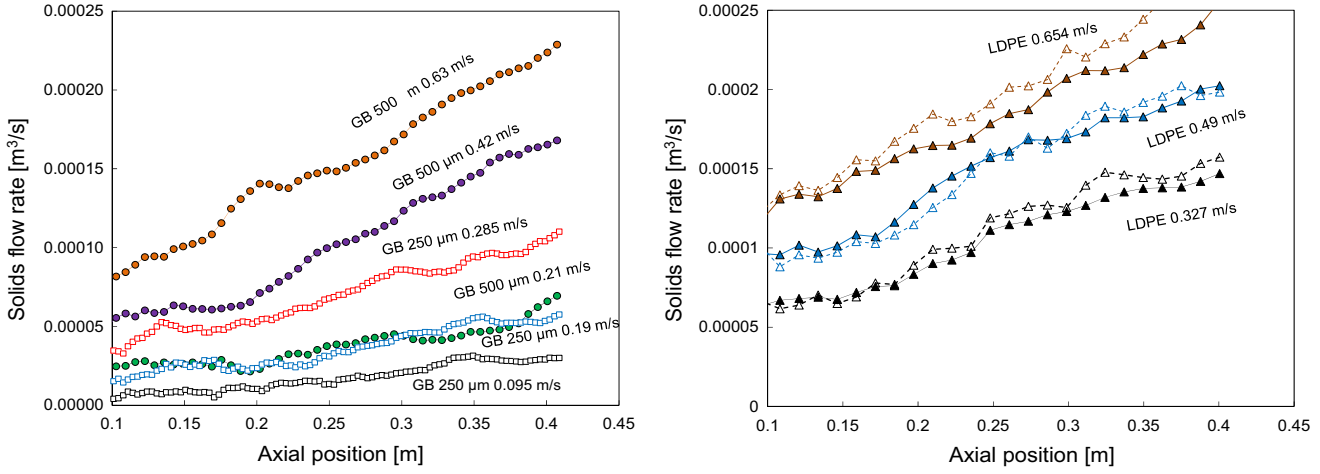

Fig. 7. Left: Solids flow rates as a function of the vertical position for glass beads of 250 μm and 500 μm at different excess gas velocities; right: Solids flow rates for LDPE particles for two different set of experiments in order to show reproducibility of the measurements.

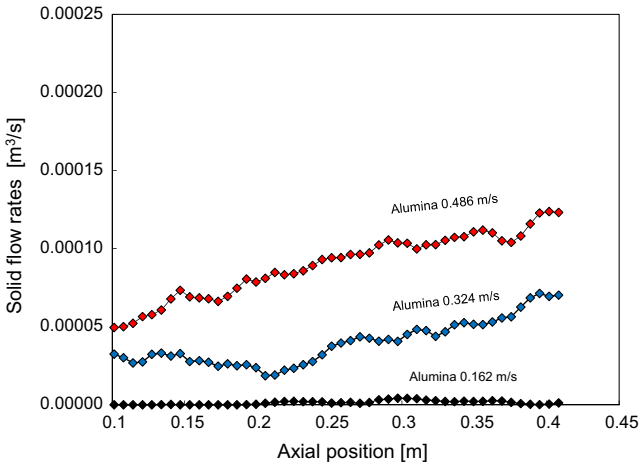

Fig. 8. Solids flow rates as a function of the vertical position for alumina particles of 500 μm diameter at different excess gas velocities.

non-spherical and they suffer from attrition. Because of this attrition and the humidity of the gas, alumina particles left a blurry white deposit on the inside front glass plate of the pseudo 2D fluidized bed. This blurry deposit does not have a large influence on the DIA post-processing technique to distinguish bubbles by pixel intensities. However, it does have a big impact on the accuracy of the PIV cross-correlation to properly detect and track the alumina particles. Henceforth, the experiments with these particles have not been considered in subsequent data analysis. A possible solution would be to use spherical alumina particles, which could significantly reduce attrition and thus reduce deposits on the glass plate.

In order to satisfy the method to determine the vertical solids fluxes using bubble properties, it is important to correlate the wake parameter with bubble characteristics at the different operating conditions. This has been done by a minimization of the fitting in order to satisfy Eq. (11). From Eq. (11), the solids fluxes are known as determined experimentally with PIV/DIA for the different cases as presented in Fig. 7. The bubble fraction (δ) corresponds to the one determined experimentally and fitted to Eq. (13), and u_b is the bubble velocity measured experimentally. All these values are time-averaged results obtained per axial position. Therefore, the unknown variable is the wake parameter, which is subsequently calculated in order to minimize the discrepancies between the predictions and the experimentally determined vertical solids fluxes. From the experimental data, if a constant value of wake parameter would be used (as commonly reported in the literature), a poor fitting between the right hand side of Eq. (11) and the experimental solids fluxes (left hand side of Eq. (11)) would be obtained. Therefore, other options have been considered in order to fit the wake parameter. As reported by Rowe and Widmer (1977), the shape of the bubbles varies as they grow leading to an increase in the wake parameter. Based on this presumption, a correlation for the wake parameter from experimental data has been proposed and is based on their exponential approach (Eq. (3)) and presented in Eq. (14). Compared to Eq. (3), the exponential value has been fitted to the experimental data, and this approach is used since it is the most likely to be accurate when working outside the experimental data range as reported by Rowe and Widmer. The coefficient was determined using the least squared method (R-squared of the fit is 0.96) and the fitting has been made on the experimental data of glass beads.

$$\alpha = 1 - e^{-4.92 d_b} \tag{14}$$

The fitted lines to the solids flow rates determined with PIV/DIA using the wake parameter from this work are shown in Fig. 9. The observed fluctuations in the solids flow rates are associated to the fact that all parameters included in the Eq. (11) are determined from the experimental data. This means that to fit the data to an expression type there is the need to use the experimental bubble rise velocity and bubble velocity determined in DIA.

It can be seen that the correlation gives a significantly better description of the solids flow rates than when assuming a constant value for the wake parameter as often used in the literature. The different descriptions of the wake parameters proposed in literature were evaluated by checking their R-squared value on the experimental data in this work and results have been summarized in Table 2.

The relation by Rowe and Widmer based on the geometry of the bubbles and fitting spheres over them to calculate the volume of the wake gives a good fit which is significantly better than assuming a constant value of 0.15. Kozanoglu and Levy (1991) used a similar geometrical approach. However, the results of their work

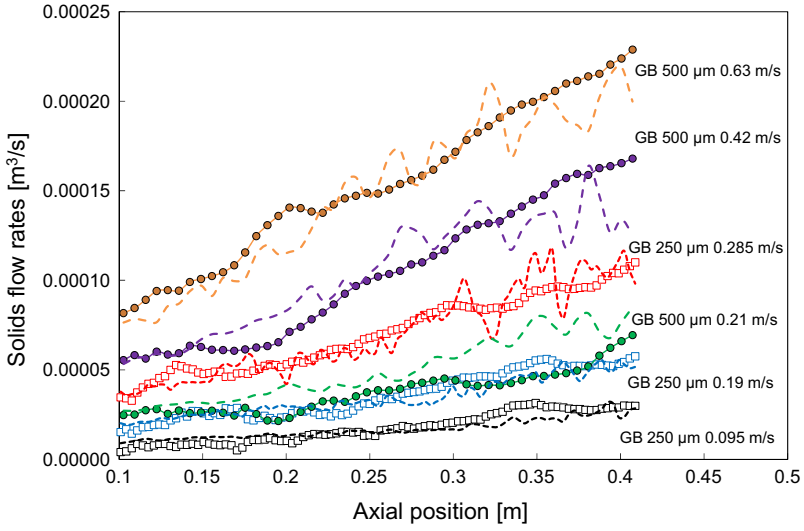

Fig. 9. Solids flow rates calculated using the bubble properties and wake parameter from this work (dashed) against solids flow rates measured from PIV/DIA (line) at different conditions.

Table 2
Wake parameters from literature and this work and their R-squared values on the experimental data in this work.

Wake parameter	Refs.	R^2
$\alpha = 0.15$	Iliuta et al. (2010); Gascon et al. (2006)	0.50
$\alpha = \left[(0.78 + 0.007 \cdot 6d_p) + \frac{3899 d_b}{d_p^{1.103}}\right]/100$	Kozanoglu and Levy (1991)	- 1.84
$\alpha = 1 - e^{-5.7 \cdot d_b}$	Rowe and Widmer (1977)	0.91
$\alpha = 1 - e^{-4.92 \cdot d_b}$	This work	0.96

gave a range of values for the bubble wake parameter without a clear relation since it was obtained for very small bubbles, even not detected in this work.

4. Discussion

To investigate the importance of the different assumptions investigated in this work, a sensitivity analysis has been carried out on a chemically reactive system using a phenomenological 1D model based on the three phase model by Kunii and Levenspiel (1968). The model assumes steady state conditions and all the correlations to solve the mass transfer and the hydrodynamics were taken from literature and can also be found in the work of Iliuta et al. (2010). The model simulates the steam methane reforming process since for this system it has been recently reported in the literature that mass transfer limitations might be expected (Spallina et al., 2016). The two main reactions taking place in the systems are presented in Eqs. (15) and (1) corresponding to the steam methane reforming and water gas shift reactions, where the kinetics have been taken from the work of Numaguchi and Kikuchi (1988). To better elucidate the influence of the assumptions on the chemical conversion, the extent of the mass transfer between the bubble and emulsion phases was reduced 10 times. Note that with modern noble-metal based catalysts much higher activities can be achieved for the steam reforming with the associated higher impact of mass transfer limitations. A summary with the operating conditions and the simulations carried out is reported in Table 3.

$$\textit{Steam Methane Reforming} \quad CH_4 + H_2O \leftrightarrow CO + 3H_2 \tag{15}$$

$$\textit{Water Gas Shift} \quad CO + H_2O \leftrightarrow CO_2 + H_2 \tag{16}$$

A sensitivity analysis on the description of the solids fluxes along the vertical direction of a reactor and the effect of the solids holdup in the bubbles is presented in this section. The effect of the presence of solids inside bubbles for a mass transfer limited system on the chemical conversion has been assessed using the phenomenological model described by Iliuta et al. (2010) and at the conditions listed in Table 3. Three different conditions have been selected, viz. 0, 2.5 (this work), and 5% of solids per bubble volume, and the results are reported in Fig. 10. It can be seen that accounting for dispersed particles in the bubbles can result in significant increase in the chemical conversion along the fluidized bed height. The additional conversion taking place already in the bubble phase increases the total fraction of the products at each vertical position, which has to be taken into account for an optimal reactor design.

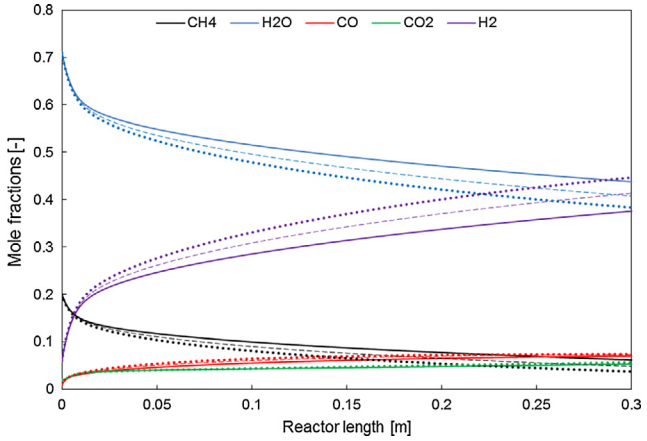

Fig. 10. Mole fractions as a function of reactor length for 0% (line), 2.5% (dashed), and 5% (dotted) of bubble solids hold-up.

Regarding the solids fluxes, first it is worth mentioning that in the open literature the solids flow rates are determined using equation Eq., which together with the bubble fraction proposed by Kunii and Levenspiel will always yield constant solids flow rates along the bed height. This would lead to a plug-flow description of the solids phase in fluidized beds since the bubble rise velocity term in the bubble fraction is cancelled out by the bubble rise velocity term in the bubble fraction (Eq. (5)). Therefore, when representing the theoretical solids flow rates expected in the experiments with the measured experimentally, an important deviation can be observed as presented in Fig. 11 for glass beads.

In most cases, the assumption of a constant wake parameter may be sufficient to predict the performance of fluidized beds where only heterogeneously catalyzed gas phase reactions take place. However, for mass transfer limited systems an accurate description of the wake parameter might become important, because it modifies the extent of the emulsion fraction and the

Table 3
List of simulations performed in phenomenological model.

Phenomenological model conditions			
Reactor dimensions and particles	Reactor height = 0.30 m Reactor diameter = 0.075 cm d_p = 250 μm ρ_p = 2400 kg/m^3		
Operating conditions	T (°C) = 700 P (bar) = 1 Superficial gas velocity = 3 times u_{mf} Inlet composition: CH_4:H_2O:H_2:CO:CO_2 = 0.2:0.7:0.05:0.025:0.025		
Sensitivity analysis	Run	Solids inside bubbles	Wake parameter (α)
	1	0	0.15
	2	0.05	0.15
	3	This work	0.15
	4	0	0.25
	5	0	This work

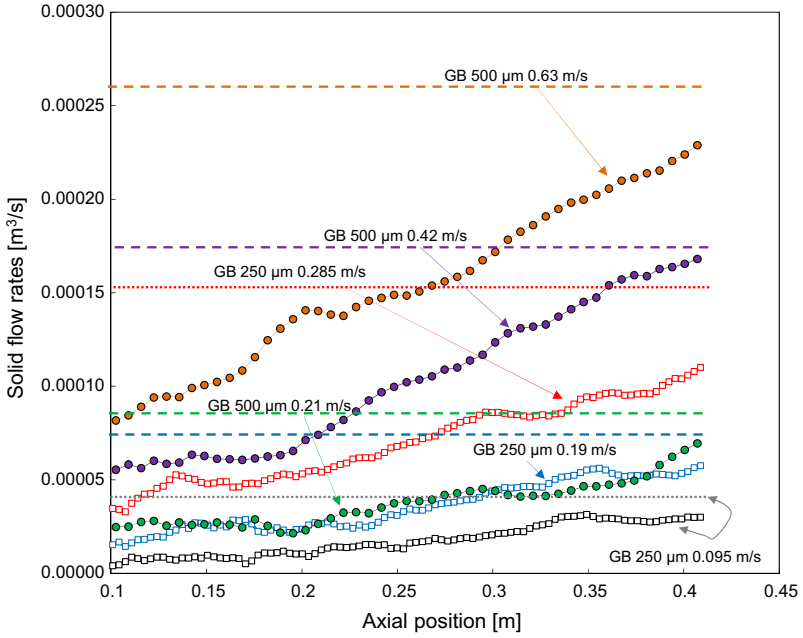

Fig. 11. Solids flow rates calculated with a constant wake parameter of 0.15 (dashed) compared to the solids flow rates determined from PIV/DIA (line) for glass beads at different excess gas velocities.

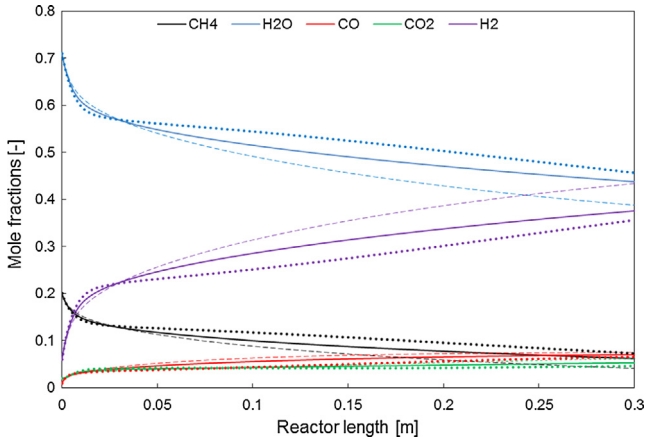

Fig. 12. Mole fractions as a function of reactor length for a wake parameter of 0.15 (line), 0.25 (dashed) and this work (dotted).

extent of gas exchange between the phases. An accurate description of the wake parameter becomes even more relevant for the case of gas-solid reactions, where the internal solids circulation is of high importance, because it determines the emulsion solids velocity. In these systems the composition of the solids phase as function of the vertical position is very important, as gas-solid reactors have inlets and outlets where fresh and used particles are introduced and extracted, where the composition of the solid phase not only affects the rate of the chemical reactions, but also where these in- and outlets should be placed.

The effect of the wake parameter correlation developed in this work on the chemical conversion compared to the case with the conventional constant wake parameter is clear from Fig. 12.

It is observed that the obtained correlation gives distinctly different mole fraction profiles compared to the case where a constant wake parameter was assumed. For instance, looking at the mole fraction profile of H_2, its initial slope is higher because the starting value of the wake fraction is lower, which implies a larger emulsion fraction that reaches equilibrium fast. Therefore, it results in a higher H_2 fraction overall. After this initial high slope, the slope of the H_2 fraction profile including the wake parameter correlation is smaller at around a reactor length of ~0.025 m. This is related to the fact that the correlation at this point gives smaller values for the wake parameter than the value assumed for the constant wake parameter case, thus reducing the amount of CH_4 transferred to the emulsion phase to react. However, the wake parameter increases with reactor length as the bubble size increases and this is reflected by the fact that the H_2 line keeps a virtually constant slope, whereas the slopes of the profiles for the constant wake parameter case decrease along the reactor length.

5. Conclusions

The validity of several important assumptions normally considered in phenomenological fluidized bed models have been investigated in detail with a PIV/DIA technique that allows the simultaneous determination of the properties of the solids and gas phases with a high temporal and spatial resolution. In particular, the amount of particles inside the bubbles has been quantified for different experimental conditions, resulting in an average amount of around 2.5–3% per bubble volume for glass beads and alumina particles, virtually independent of the excess gas velocity.

Subsequently, the internal solid circulation has been investigated by developing novel methods to measure bubble and wake fractions in the bed. First, it has been found that the theoretical correlation for the bubble fraction proposed in the literature tends to overestimate the amount of bubble phase present in the bed, i.e. a visual bubble flow rate parameter significantly smaller than unity. By the combination of information from the solids phase (solids fluxes) and bubble properties (bubble fraction, bubble diameter and bubble rise velocity), an empirical correlation has been proposed, which relates the amount of solids moving upwards with the bubble phase as a function of the bubble diameter, which is related to the bubble shape. The equation as developed solves the internal mass balance for the solids phase and can be applied for Geldart B particles in fluidized beds. The novel methods developed in this study have the advantage that are based

on the real dynamics of the freely bubbling fluidized bed, as opposed to selecting arbitrary bubbles and fitting spheres/circles onto them based on geometrical assumptions. In this work, the wake parameter has been calculated based on experimental data to determine the solids flow rates. Furthermore, it has been observed that the new correlation to determine the wake parameter is able to solve the internal mass balance for the solids phase in the fluidized bed and it has been shown to give a proper description of the solids flow rates. Finally, the influence of the new data and correlations has been assessed for the heterogeneously catalyzed methane steam reforming with mass transfer rate limitations. The results confirm that for these systems the improved correlations are required to enhance the description of the hydrodynamics and mass transfer in fluidized bed reactors.

Acknowledgements

NWO/STW is acknowledged for the financial support through the VIDI project number 12365.

References

Agarwal, P.K., Hull, A.S., Lim, K.S., 1997. Chapter 12 - Digital image analysis techniques for the study of bubbling fluidized beds. In: Chaouki, J., Larachi, F., Duduković, M.P. (Eds.), Non-Invasive Monit. Multiph. Flows. Elsevier Science B. V., Amsterdam, pp. 407–454. http://dx.doi.org/10.1016/B978-044482521-6/50013-9.

Andreux, R., Chaouki, J., 2008. Behaviors of the bubble, cloud, and emulsion phases in a fluidized bed. AIChE J. 54, 406–414. http://dx.doi.org/10.1002/aic.11390.

Andreux, R., Gauthier, T., Chaouki, J., Simonin, O., 2005. New description of fluidization regimes. AIChE J. 51, 1125–1130. http://dx.doi.org/10.1002/aic.10380.

Aoyagi, M., Kunii, D., 1974. Importance of dispersed solids in bubbles for exothermic reactions in fluidized beds. Chem. Eng. Commun. 1, 191–197. http://dx.doi.org/10.1080/00986447408960430.

Bokkers, G.A., Van Sint Annaland, M., Kuipers, J.A.M., 2004. Mixing and segregation in a bidisperse gas-solid fluidised bed: a numerical and experimental study. Powder Technol. 140, 176–186. http://dx.doi.org/10.1016/j.powtec.2004.01.018.

Boyce, C.M., Davidson, J.F., Holland, D.J., Scott, S.A., Dennis, J.S., 2014. The origin of pressure oscillations in slugging fluidized beds: comparison of experimental results from magnetic resonance imaging with a discrete element model. Chem. Eng. Sci. 116, 611–622. http://dx.doi.org/10.1016/j.ces.2014.05.041.

Broadhurst, T.E., Becker, H.A., 1975. Onset of fluidization and slugging in beds of uniform particles. AIChE J. 21, 238–247. http://dx.doi.org/10.1002/aic.690210204.

Buist, K.A., van der Gaag, A.C., Deen, N.G., Kuipers, J.A.M., 2014. Improved magnetic particle tracking technique in dense gas fluidized beds. AIChE J. 60, 3133–3142. http://dx.doi.org/10.1002/aic.14512.

Chaouki, J., Larachi, F., Dudukovic, M.P., 1997. Noninvasive tomographic and velocimetric monitoring of multiphase flows. Ind. Eng. Chem. Res. 5885, 4476–4503. http://dx.doi.org/10.1021/ie970210t.

Cui, H., Mostoufi, N., Chaouki, J., 2000. Characterization of dynamic gas-solid distribution in fluidized beds. Chem. Eng. J. 79, 133–143. http://dx.doi.org/10.1016/S1385-8947(00)00178-9.

Davidson, J.F., Harrison, D., 1963. Fluidised particles. Cambridge University Press, New York.

de Jong, J.F., Odu, S.O., Van Buijtenen, M.S., Deen, N.G., Van Sint Annaland, M., Kuipers, J.A.M., 2012. Development and validation of a novel Digital Image Analysis method for fluidized bed Particle Image Velocimetry. Powder Technol. 230, 193–202. http://dx.doi.org/10.1016/j.powtec.2012.07.029.

Dijkhuizen, W., Bokkers, G.A., Deen, N.G., van Sint Annaland, M., Kuipers, J.A.M., 2007. Extension of PIV for measuring granular temperature field in dense fluidized beds. AIChE J. 53, 108–118. http://dx.doi.org/10.1002/aic.11044.

Duursma, G.R., Glass, D.H., Rix, S.J.L., Yorquez-Ramirez, M.I., 2001. PIV investigations of flow structures in the fluidised bed freeboard region. Powder Technol. 120, 2–11. http://dx.doi.org/10.1016/S0032-5910(01)00340-0.

Fraguío, M.S., Cassanello, M.C., Larachi, F., Limtrakul, S., Dudukovic, M., 2007. Classifying flow regimes in three-phase fluidized beds from CARPT experiments. Chem. Eng. Sci. 62, 7523–7529. http://dx.doi.org/10.1016/j.ces.2007.08.039.

Gascon, J., Tellez, C., Herguido, J., Jakobsen, H.A., Menendez, M., 2006. Modeling of fluidized bed reactors with two reaction zones. AIChE J. 52, 3911–3923. http://dx.doi.org/10.1002/aic.

Goldschmidt, M.J.V., Link, J.M., Mellema, S., Kuipers, J.A.M., 2003. Digital image analysis measurements of bed expansion and segregation dynamics in dense gas-fluidised beds. Powder Technol. 138, 135–159. http://dx.doi.org/10.1016/j.powtec.2003.09.003.

He, C., Bi, X.T., Grace, J.R., 2015. Monitoring electrostatics and hydrodynamics in gas-solid bubbling fluidized beds using novel electrostatic probes. Ind. Eng. Chem. Res. 54, 8333–8343. http://dx.doi.org/10.1021/acs.iecr.5b01512.

Hilligardt, K., Werther, J., 1986. Local bubble gas hold-up and expansion of gas/solid fluidized beds. Ger. Chem. Eng. 9, 215–221 https://www.scopus.com/inward/record.uri?eid=2-s2.0-0022513322&partnerID=40&md5=967b77f73fd94b39dacf4452d1d55c9d.

Hiraki, I., Yoshida, K., Kunii, D., 1965. Behaviour of bubbles in Tw-dimensional fluidized bed. Kugaku Kogaku Ronbunshu. 29, 846–851.

Horio M., Wen C.Y., 1977. An assessment of fluidized-bed modelling, in: Fluid. Theor. Appl., American Institute of Chemical Engineers, New York, pp. 9–21.

Iliuta, I., Tahoces, R., Patience, G.S., Rifflart, S., Luck, F., 2010. Chemical-looping combustion process: Kinetics and mathematical modeling. AIChE J. 56, 1063–1079. http://dx.doi.org/10.1002/aic.11967.

Kato, K., Wen, C.Y., 1969. Bubble assemblage model for fluidized bed catalytic reactors. Chem. Eng. Sci. 24, 1351–1369. http://dx.doi.org/10.1016/0009-2509(69)85055-4.

Kobayashi, H., Arai, F., Chiba, T., 1965. Behaviours of bubbles in gas-solid fluidized-bed. Kugaku Kogaku Ronbunshu. 29, 858–863.

Kozanoglu, B., Levy, E.K., 1991. Wake fractions of small bubbles in gas fluidized beds. Powder Technol. 68, 285–286. http://dx.doi.org/10.1016/0032-5910(91)80054-M.

Kunii, D., Levenspiel, O., 1968. Bubbling bed model. Ind. Eng. Chem. Fundam. 7, 446–452.

Kunii D., Levenspiel O., 1991. Fluidization engineering, second ed.

Laverman, J., Roghair, I., van Sint Annaland, M., Kuipers, J.a.M., 2008. Investigation into the hydrodynamics of gas–solid fluidized beds using particle image velocimetry coupled with digital image analysis. Can. J. Chem. Eng. 86, 523–535.

Laverman, J.A., Fan, X., Ingram, A., Annaland, V.S.M., Parker, D.J., Seville, J.P.K., Kuipers, J.A.M., 2012. Experimental study on the influence of bed material on the scaling of solids circulation patterns in 3D bubbling gas-solid fluidized beds of glass and polyethylene using positron emission particle tracking. Powder Technol. 224, 297–305. http://dx.doi.org/10.1016/j.powtec.2012.03.011.

Lim, K.S., Agarwal, P.K., O'neill, B.K., 1990. Measurement and modelling of bubble parameters in a two-dimensional gas-fluidized bed using image analysis. Powder Technol. 60, 159–171. http://dx.doi.org/10.1016/0032-5910(90)80140-T.

Lim, C.N., Gilbertson, M.A., Harrison, A.J.L., 2007. Bubble distribution and behaviour in bubbling fluidised beds. Chem. Eng. Sci. 62, 56–69. http://dx.doi.org/10.1016/j.ces.2006.08.034.

Link, J.M., Cuypers, L.A., Deen, N.G., Kuipers, J.A.M., 2005. Flow regimes in a spout–fluid bed: A combined experimental and simulation study. Chem. Eng. Sci. 60, 3425–3442. http://dx.doi.org/10.1016/j.ces.2005.01.027.

Maurer, S., Wagner, E.C., Schildhauer, T.J., van Ommen, J.R., Biollaz, S.M.A., Mudde, R. F., 2015. X-ray measurements of bubble hold-up in fluidized beds with and without vertical internals. Int. J. Multiph. Flow. 74, 118–124. http://dx.doi.org/10.1016/j.ijmultiphaseflow.2015.03.009.

Mudde, R.F., Schulte, H.B.M., van den Akker, H.E.A., 1994. Analysis of a bubbling 2-D gas-fluidized bed using image processing. Powder Technol. 81, 149–159.

Müller, C.R., Davidson, J.F., Dennis, J.S., Hayhurst, A.N., 2007. A study of the motion and eruption of a bubble at the surface of a two-dimensional fluidized bed using Particle image velocimetry (PIV). Ind. Eng. Chem. Res. 46, 1642–1652. http://dx.doi.org/10.1021/ie0611397.

Numaguchi, T., Kikuchi, T., 1988. Intrinsic kinetics and design simulation in a complex reaction network: Steam-Methane Reforming. Chem. Eng. Sci. 43, 2295–2301.

Pallarès, D., Johnsson, F., 2006. A novel technique for particle tracking in cold 2-dimensional fluidized beds—simulating fuel dispersion. Chem. Eng. Sci. 61, 2710–2720. http://dx.doi.org/10.1016/j.ces.2005.11.030.

Rowe, P.N., Partridge, B.A., 1965. An x-ray study of bubbles in fluidised beds. Trans. Inst. Chem. Eng. 43, 157.

Rowe, P.N., Widmer, A.J., 1977. Variation in shape with size of bubbles in fluidised beds. Chem. Eng. Sci. 28, 980–981.

Shen, L., Johnsson, F., Leckner, B., 2004. Digital image analysis of hydrodynamics two-dimensional bubbling fluidized beds. Chem. Eng. Sci. 59, 2607–2617. http://dx.doi.org/10.1016/j.ces.2004.01.063.

Spallina, V., Pandolfo, D., Battistella, A., Romano, M.C., Van Sint Annaland, M., Gallucci, F., 2016. Techno-economic assessment of membrane assisted fluidized bed reactors for pure H2 production with CO2 capture. Energy Convers. Manag. 120, 257–273. http://dx.doi.org/10.1016/j.enconman.2016.04.073.

Toei, R., Matsuno, R., Kojima, H., Nagai, Y., Nakagawa, K., Yu, S.I., 1965. Behaviours of bubbles in gas-solid fluidized-bed. Kugaku Kogaku Ronbunshu. 29, 851–857.

van Deemter, J.J., 1961. Mixing and contacting in gas-solid fluidized beds. Chem. Eng. Sci. 13, 143–154. http://dx.doi.org/10.1016/0009-2509(61)80005-5.

van Ommen, J.R., Sasic, S., van der Schaaf, J., Gheorghiu, S., Johnsson, F., Coppens, M.-O., 2011. Time-series analysis of pressure fluctuations in gas–solid fluidized beds – a review. Int. J. Multiph. Flow. 37, 403–428. http://dx.doi.org/10.1016/j.ijmultiphaseflow.2010.12.007.

Weber, J.M., Mei, J.S., 2013. Bubbling fluidized bed characterization using electrical capacitance volume tomography (ECVT). Powder Technol. 242, 40–50. http://dx.doi.org/10.1016/j.powtec.2013.01.044.

Westerweel, J., 1997. Fundamentals of digital particle image velocimetry. Meas. Sci. Technol. 8, 1379–1392. http://dx.doi.org/10.1088/0957-0233/8/12/002.

Yang W.-C., Handbook of fluidization and fluid-particles systems, 2003.